J Solid State Electrochem (2005) 9: 823–835
DOI 10.1007/s10008-005-0019-5

ORIGINAL PAPER

G. Inzelt · Z. Puskás · K. Németh · I. Varga

Electrochemically induced transformations of ruthenium(III) trichloride microcrystals in salt solutions

Received: 3 May 2005 / Revised: 9 May 2005 / Accepted: 19 May 2005 / Published online: 12 August 2005

Abstract Ruthenium (III) trichlorid solid crystals have been mechanically attached to gold surfaces and studied by cyclic electrochemical quartz crystal microbalance measurements in the presence of aqueous solutions of different concentrations containing M^+Cl^-, where $M^+ = H^+$, Li^+, Na^+, K^+, Rb^+, Cs^+. The $RuCl_3$ and the complexes formed during the electrochemical transformations show two or more reduction and reoxidation pairs of waves, depending on the experimental conditions (concentration, scan rate, and potential range). The voltammetric peaks are shifted into the direction of higher potentials with increasing electrolyte concentrations except at very high concentrations when the peaks belong to the first reduction/reoxidation processes move oppositely. The mass change was reversible, during reduction mass increase, while during oxidation mass decrease occurred at medium electrolyte concentrations in two, more or less distinct steps. At high or low concentrations the mass excursions are more complex involving different mass increase/decrease regions as a function of potential which vary with the potential range of the measurements. The peak potentials and the electrochemical activity strongly depend on the nature of the cations and pH. It is related to the formation of complexes in different compositions. The mass change decreases with increasing electrolyte concentrations attesting the important role of the water activity and the transport of solvent molecules. It was concluded that in dilute solutions during the first reduction step M^+ ions enter the surface layer. The strongly hydrated Li^+ ions transfer water molecules into the microcrystals, while simultaneously with the incorporation of K^+, Rb^+, and Cs^+ ions H_2O molecules leave the surface layer. The opposite transport of ions and solvent molecules occur during oxidation. In the course of further reduction the incorporation of all ions studied except that of Cs^+ ions is accompanied with water sorption. The number of sorbed water molecules is proportional to the hydration number of these ions. A reaction scheme is proposed in which $M^+_{m-3}[Ru^{III}Cl_m(H_2O)_n]^{3-m} \cdot xH_2O$ ($m \geq 3$) and $[Ru^{III}Cl_m(H_2O)_n]^{3-m}(Cl^-)_{3-m} \cdot xH_2O$ ($m \leq 3$) type complexes are reduced to the respective – or depending on the electrolyte concentration higher or lower – Ru(II)-chloro complexes resulting in mixed valence compounds (phases). Taking into account the layered structure of $RuCl_3$ the electrochemical reduction can be explained as an intercalation reaction in that mixed valence intercalation phases with a general formula $M_x^+(H_2O)_y[RuCl_3]^{x-}$ are formed from $RuCl_3 \cdot x\ H_2O$. The reduction/reoxidation waves are related to the redox transformations of Ru(III) to Ru(II) sites, while the composition of the polynuclear complexes and the structure of microcrystals change.

Keywords Ruthenium(III) chloride · Microcrystals · Solid state electrochemistry · Intercalation · Electrochemical quartz crystal microbalance

Introduction

Ruthenium and its compounds have been widely used especially in the field of homogeneous and heterogeneous catalysis including electrocatalysis and photocatalysis [1–8]. Their catalytic activity regarding different oxidation and reduction as well as other reactions (e.g., dimerization and polymerization) strongly depends on their oxidation state (ruthenium displays ten oxidation states), and on the media used because of the formation of different simple and polynuclear complexes. Due to the versatility of ruthenium compounds this field has not been fully explored, yet. It is especially interesting to gain a deeper insight into the redox transformations of

Presented at the 4th Baltic Conference on Electrochemistry, Greifswald, March 13–16, 2005.

G. Inzelt (✉) · Z. Puskás · K. Németh · I. Varga
Department of Physical Chemistry, Eötvös Loránd University, Pázmány Péter sétány 1/A, 1117 Budapest, Hungary
E-mail: inzeltgy@para.chem.elte.hu
Tel.: +36-1-2090555
Fax: +36-1-3722548

ruthenium compounds in solid state. Ruthenium containing polynuclear hexacyanometallate modified electrodes [9–12] were studied recently in order to find useful systems for practical applications in such areas as electroanalysis, chemical sensing, electrocatalysis, electrochromic, and electroluminescence displays etc.

The technique of voltammetry α-RuClof immobilized microparticles (VIM) [13–15] has also been applied to study ruthenium complexes [16, 17]. We have started studying the redox transformations of α-$RuCl_3$ microcrystals attached to a gold electrode by combined VIM and piezoelectric microgravimetry at an electrochemical quartz crystal microbalance (EQCM) [18]. These microcrystals are insoluble in water and organic solvents which are connected with their structure in solid state [1–4, 19, 20]. α-$RuCl_3$ belongs to a group of layered transition metal halides, where one hexagonal sheet of Ru atoms is sandwiched between two hexagonal sheets of chlorine. However, one-third of the Ru atoms are missing in the metallic sheet. Within a sandwich the bonding is mainly of ionic character (the coordination around the metal atom is octahedral), whereas the van der Waals bonding is responsible for the stacking between the sandwiches. A recent study of the electronic properties of the low-spin compound suggested that $RuCl_3$ may be classified as a Mott-Hubbard insulator (unconventional semiconductor) [21, 22] in which the band gap corresponds to intercationic d–d transitions [19, 20]. The conductivity energy gap is around 1 eV. There are still some contradictions regarding the interpretation of the transport properties of this material, and a band conduction for the description of its electrical properties cannot be excluded [19, 20]. It has been found that the crystals remain insoluble during cycling in a wide potential range in acidic media, while showing interesting redox transformations accompanied with ionic and solvent exchange processes. Therefore, it is possible to tune the oxidation state of the ruthenium in the complexes formed and to prepare different surface compounds. It is expected that these microcrystals have specific catalytic activity. According to our previous experiences the electrochemical transformations of $RuCl_3$ strongly depend on the nature and composition of the solution including its acidity. Consequently, it is useful to investigate the behavior of these microcrystals in neutral media. In this paper, we report the new findings on the potential induced changes of α-$RuCl_3$ attached to gold and platinum in salt solutions of different concentrations.

Experimental

Black-colored $RuCl_3$ microcrystals, HCl, LiCl, NaCl, KCl, RbCl, and CsCl (Merck, analytical grade) were used as received. Doubly distilled water was used. Ten megahertz AT-cut crystals coated with gold were used in the EQCM measurements. The detailed description of the apparatus and its calibration have been published in our previous papers [18, 23–25]. The geometrical and piezoelectrically active area of the working electrode was 0.4 cm^2. A Pt wire was used as a counter electrode. The reference electrode was a saturated sodium calomel electrode (SCE). All potentials are referred to the SCE. The microcrystals were attached to the gold surface by wiping the electrode with a cotton swab containing the material [15, 18, 23–25], and then making use of a drop of distilled tetrahydrofuran (THF) or water the microcrystals were fixed. Although $RuCl_3$ was found to be insoluble in THF or in water, by the help of this procedure, the crystals can be ''glued'' to the metal. In separate experiments it was checked that the behavior of $RuCl_3$ remains unaltered and liquid added evaporates completely. This method of preparing the electrode produces a randomly distributed ensemble of microcrystals on the gold, however, the distribution of microcrystals was more or less uniform. Although the requirements (uniform and homogeneous surface layer) for the application of Sauerbrey equation are not perfectly met, on the basis of measured frequency values (Δf) a rough estimation can be done. The relative values of Δf obtained for the incorporation of different ions and solvent molecules, however, should be approximately correct. Therefore, Sauerbrey equation [25] was used for the estimation of the surface mass changes (Δm) from the frequency changes (Δf) with an integral sensitivity ($C_f = (1.9 \pm 0.2) \times 10^8$ Hz cm^2 g^{-1}) that was determined in separate experiments [25]. The amount of $RuCl_3$ immobilized on the surface (0.5–15 μg) was estimated by measuring the crystal frequency before and after the deposition in dry state. Solutions of different concentrations of MCl salts, where M = Li, Na, K, Rb, and Cs were used. The pH dependence has been studied in the presence of 0.1 mol dm^{-3} LiCl + x mol dm^{-3} HCl. The measurements were carried out at 25°C.

All solutions were purged with oxygen-free argon and an inert gas blanket was maintained throughout the experiments.

An Elektroflex 453 potentiostat and an Universal Frequency Counter TR-5288 connected with an IBM personal computer were used for the control of the measurements and for the acquisition of the data.

$RuCl_3$ microcrystals before and after potentiostatic reduction at different potentials were investigated by the total reflection X-ray fluorescence (TXRF) spectrometry. A TXRF spectrometer (EXTRA II, Rich. Seifert and Co., Ahrensburg, Germany) was used to determine the element concentrations. The line-focused W or Mo-tubes were operated at 25 kV (60 mA) and 50 kV (30 mA), respectively. An energy dispersive Si(Li)-detector (QX 2000, Oxford Instruments, England) was used. The integration time was 300–3,000 s. The apparatus was calibrated by using KCl and Ru. Other details of the measurements have been published previously [26, 27]. The samples were investigated on the gold substrate and also after removal from the electrode in powder form. The electrodes were carefully rinsed and dried after the electrochemical experiments. In the case of thick samples the outer part of the microcrystal layer

and the thin layer strongly adhered to the gold surface have been detached and studied, separately.

Results and discussion

The effect of the nature of the electrolyte

The behavior of the surface layer is considerably affected by the nature of the cations. Typical sets of voltammograms and the simultaneously obtained EQCM frequency curves in the presence of 0.2 mol dm^{-3} LiCl, NaCl, KCl, RbCl, and CsCl, respectively, are presented in Figs. 1 and 2. Depending on the experimental conditions (concentration, scan rate, potential range) at least two pairs of waves develop in the potential interval from 0.75 V to −0.5 V versus SCE. (Above ca. 0.75 V, a new oxidation process starts, while below −0.5 V, hydrogen evolution occurs.)

At starting potentials (0.7 V or 0.75 V) practically no current flows and the frequency is constant, however, between cycles, a delay time (0.5–3 min) is necessary to reach the stable state. The peak potential of the first reduction wave (I) in the presence of Li^+, Na^+ or K^+ ions is only slightly sensitive to the nature of cations ($0.225\ V < E^{I}_{pc} < 0.236\ V$), however, the electroactivity of the microcrystals substantially increase in order of $Li^+ < Na^+ < K^+ < Cs^+ < Rb^+$. The much lower electroactivity in the case of Li^+ ions can be explained by the incomplete reoxidation at a concentration of 0.2 mol dm^{-3} (see the concentration dependence later). Such type of cation dependence has been found for several insertion and intercalation processes [13]. For the metal hexacyanoferrate (MeHCFe) layers (Me = Fe [28], Ni [29–32], Pd [33], Cu [34, 35], Co [36], In [37] etc.) the kinetic effect has mostly been explained in terms of the effective diameter of the hydrated or partially dehydrated cations, which diffuse through the channels of the two or three dimensional network or move into the interlayer space. Usually the fastest transport rate was observed in the case of K^+ ions. This phenomenon can be interpreted on the basis of the effective size of the diffusing ions, since K^+ ions are much less hydrated than Li^+ or Na^+ ions, but the size of K^+ ions is much

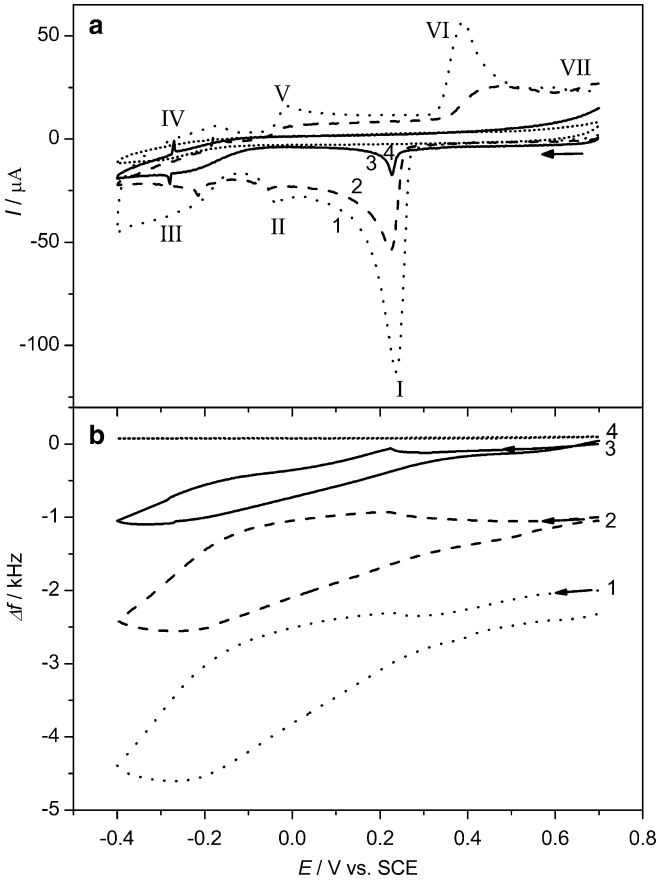

Fig. 1 Cyclic voltammograms **a** and the simultaneously detected EQCM frequency responses **b** for $RuCl_3$ microcrystals attached to a gold surface in the presence of 0.2 mol dm^{-3} solutions of KCl(*1*), NaCl(*2*), and LiCl(*3*), respectively. *Curves* (*4*) were obtained for the pure gold electrode in contact with 0.2 mol dm^{-3} LiCl. Scan rate: 5 mV s^{-1}. Starting potential was 0.7 V

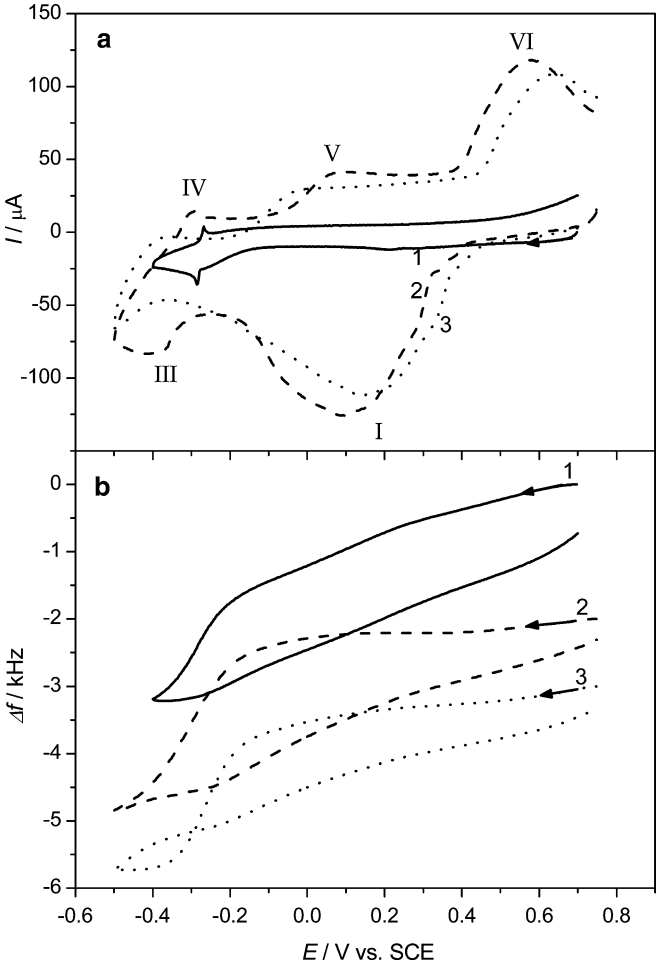

Fig. 2 Cyclic voltammograms **a** and the respective EQCM curves **b** for $RuCl_3$ microcrystals in the presence of 0.2 mol dm^{-3} solutions of LiCl *1*, RbCl (*2*), and CsCl (*3*). Scan rate: 5 mV s^{-1}

smaller than that of Rb^+ or Cs^+ ions. The dependence of the peak potentials on the nature of the cations is related to the standard free energy change of the transfer of the intercalated ions as well as to the structural change of the host matrix. The former effect is relatively small, e.g., for MeHCFe systems it is some 10 mV [13]. The variation of E_p values for the $RuCl_3$ systems reflects also the change of the hexagonal lattice parameters of α-$RuCl_3$ and of hydrated phases obtained by reduction in the presence of different electrolytes. It was found that there is a substantial change of the interlayer spacing (d). The change $\Delta d = d–d$ ($RuCl_3$) is very sensitive to the nature of cations, Δd/pm = 540.1 (Li^+), 566.5 (Na^+), 296.7 (K^+), 293.3 (Rb^+), and 301.3 (Cs^+) [38, 39]. A small wave (II) appears at ca. −0.035 V (KCl) and at −0.055 V (NaCl), respectively, while for LiCl this process is silent in the cyclic voltammograms, however, the frequency continuously decreases in this potential range for all the three electrolytes.

A rather spectacular, sharp pair of waves with small peak separations (ΔE_p = 10–30 mV) develop at low potentials (wave III—reduction and wave IV—oxidation), which is accompanied with substantial mass changes. The position of these peaks depends on the nature of cations. The reversible redox process takes place at most negative potentials in the case of Li^+ ions, E_{pc}(III) = −0.279 V and E_{pa}(IV) = −0.27 V, while for Na^+ and K^+ in the potential region between − 0.215 V and − 0.171 V at c = 0.2 mol dm^{-3}. The intermediate peak (V) during the reoxidation appears in the case of KCl, which is only a shoulder for NaCl, and no such wave for LiCl, however, for all the three electrolytes a continuous mass decrease can be observed in this potential range.

The reoxidation proceeds at wave VI, the frequency value returns to its starting value at low sweep rates. E_{pa}(VI) depends on the nature and the concentration (see later) of the electrolytes. The reoxidation is the easiest in the presence of KCl, while at 0.2 mol dm^{-3} concentration it is incomplete in LiCl solution. As seen in Fig. 1 (curves 1 and 2) that beside the main wave a smaller peak (VII) also develops. Somewhat surprisingly, in the presence of bulkier Rb^+ or Cs^+ ions the electroactivity (the charge consumed, Q) becomes even higher (Fig. 2). A very broad peak I develops and its peak potential shifts into the direction of lower potentials in comparison with that of the smaller ions. Waves III and IV are not sharp, either, similarly to that in K^+ containing solutions, and wave V also appears during the reoxidation. The reoxidation is incomplete at peak VI, the peak potentials are higher than those obtained in KCl or NaCl solutions, however, the reoxidation is still much easier than in LiCl electrolyte of the same concentration. Nevertheless, the character of the mass change is similar to those observed for other electrolytes.

It is of importance to clarify whether the exchanges of the electrolytes have a permanent effect on the electrochemical behavior of the microcrystals or not. Because the most drastic changes occur in the presence of Rb^+ or Cs^+ ions in comparison with ions of smaller size, two experiments have been carried out. First, RbCl was added gradually to the solution of 0.2 mol dm^{-3} of NaCl. The changes of the voltammograms and the frequency–potential functions are shown in Fig. 3. As seen, RbCl affects both functions in the way described previously. Figure 4 shows the cyclic voltammograms and the Δf–E curves obtained in the presence of 0.2 mol dm^{-3} LiCl before replacing LiCl by NaCl then by RbCl (curve 1) and after the experiments shown in Fig. 3 (curve 2), respectively. As seen in Fig. 4 the character of the responses in the presence of LiCl remained practically the same, however, a relatively high increase of the electrochemical activity and slight decrease in the frequency change can be observed.

The apparent molar mass (M_{app}) of the species exchanged during the electrochemical transformations can be calculated by a simple relationship

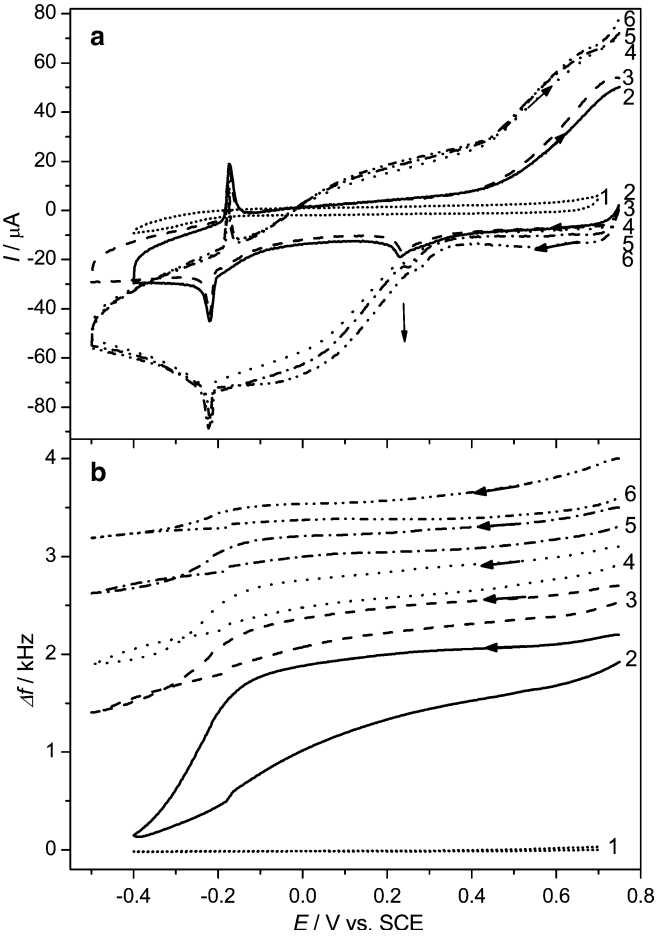

Fig. 3 The changes of the voltammograms **a** and the simultaneously obtained frequency responses **b** for an Au|$RuCl_3$ electrode after gradual addition of RbCl to 0.2 mol dm^{-3} NaCl solution. RbCl concentrations: (*2*) 0, (*3*) 0.01, (*4*) 0.056, (*5*) 0.075, and (*6*) 0.16 mol dm^{-3}. *Curves* (*1*) were obtained for the pure gold electrode in 0.2 mol dm^{-3} NaCl background electrolyte. Scan rate: 5 mV s^{-1}

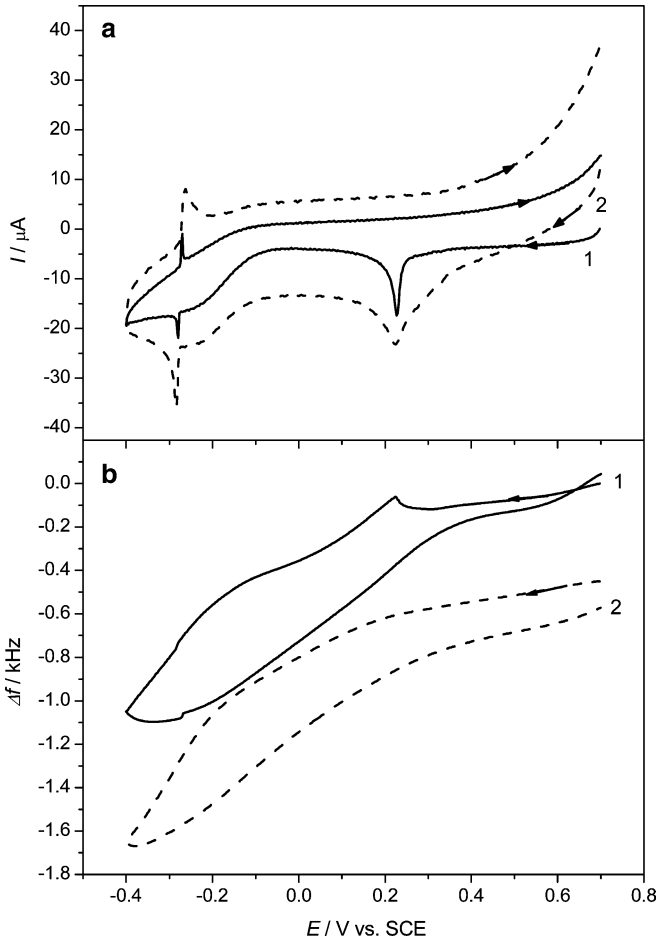

Fig. 4 The cyclic voltammograms **a** and the frequency responses **b** obtained for an Au|$RuCl_3$ electrode in 0.2 mol dm^{-3} LiCl solutions before (*1*) and after (*2*) the experiments shown in Fig. 3. Scan rate: 5 mV s^{-1}

$$M_{app} = \frac{\Delta f A n F}{C_f Q},$$

where Δf is the measured frequency change, A is the geometric area of the electrode which is equal to the piezoelectrically active area, n is the number of electron exchanged in the reaction ($n = 1$ is considered), F is the Faraday constant, C_f is the integral sensitivity, and Q is the charge consumed during the respective reaction. If only a single charged species, usually as a counterion to maintain the electroneutrality within the layer, is exchanged, M_{app} is equal to the molar mass of this ion. However, in many cases solvent sorption/desorption accompany this process as well as, co-ion sorption/desorption may also occur. Furthermore, the phase transition, surface structural changes causing strain in the surface layer, can lead to anomalously large frequency changes (M_{app} values) [17, 40, 41].

In our case all these effects should be considered since (1) M_{app} values calculated showed no correlation with M_{cation} which is expected to enter the microcrystals during reduction, (2) anomalously large M_{app} values

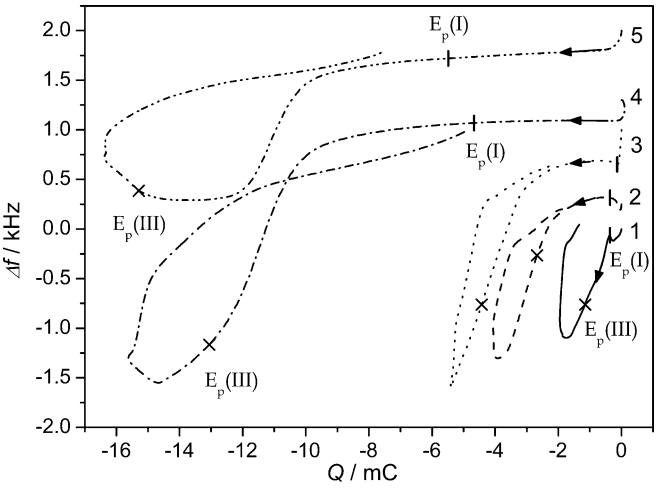

Fig. 5 The frequency changes (Δf) versus charge consumed (Q) curves as a function of nature of the electrolytes: (*1*) LiCl, (*2*) NaCl, (*3*) KCl, (*4*) RbCl, and (*5*) CsCl for an Au|$RuCl_3$ electrode. Waves I and III are indicated on the plots. Electrolyte concentration: 0.2 mol dm^{-3}. Scan rate: 5 mV s^{-1}

were derived, and (3) phase transitions are expected (the rather large separation of waves I and VI relates to the additional energy, which is needed to create the solid/solid interface between the reduced and unreduced forms [13, 17, 42, 43]). At relatively low electrolyte concentrations the $\Delta f - E$ curves (Figs. 1, 2) and the $\Delta f - Q$ curves (Fig. 5) exhibit more or less similar pictures for all electrolytes studied and their characteristic features do not depend on the previous experiments, however, the actual M_{app} values that can be determined are strongly affected by the prehistory of the samples (see Fig. 4).

It is seen in Fig. 5 (and also in Figs. 1, 2, and 4 which data were used to construct Fig. 5) that in dilute solutions the mass increase started after wave I, although already substantial charge had been injected. Just before the frequency decrease for a short period, a frequency increase occurs. In the case of organic microcrystals, such phenomena have been assigned to the phase transformation [44]. The mass change becomes much higher in the potential region of peak III and similarly varies M_{app}. The M_{app} values calculated from the measurements shown in Figs. 1 and 2 (and Fig. 5) are compiled in Table 1.

Table 1 The apparent molar mass of the exchanged species in the presence of different electrolytes

Electrolyte	M_{app} (g mol^{-1})	
	After Peak I	After peak III
LiCl	80, 275, 550	125, 145, 329
NaCl	22	204
KCl	15	182
RbCl	4	122
CsCl	4	126

Solution concentration: 0.2 mol dm^{-3}. Scan rate:5 mV s^{-1}

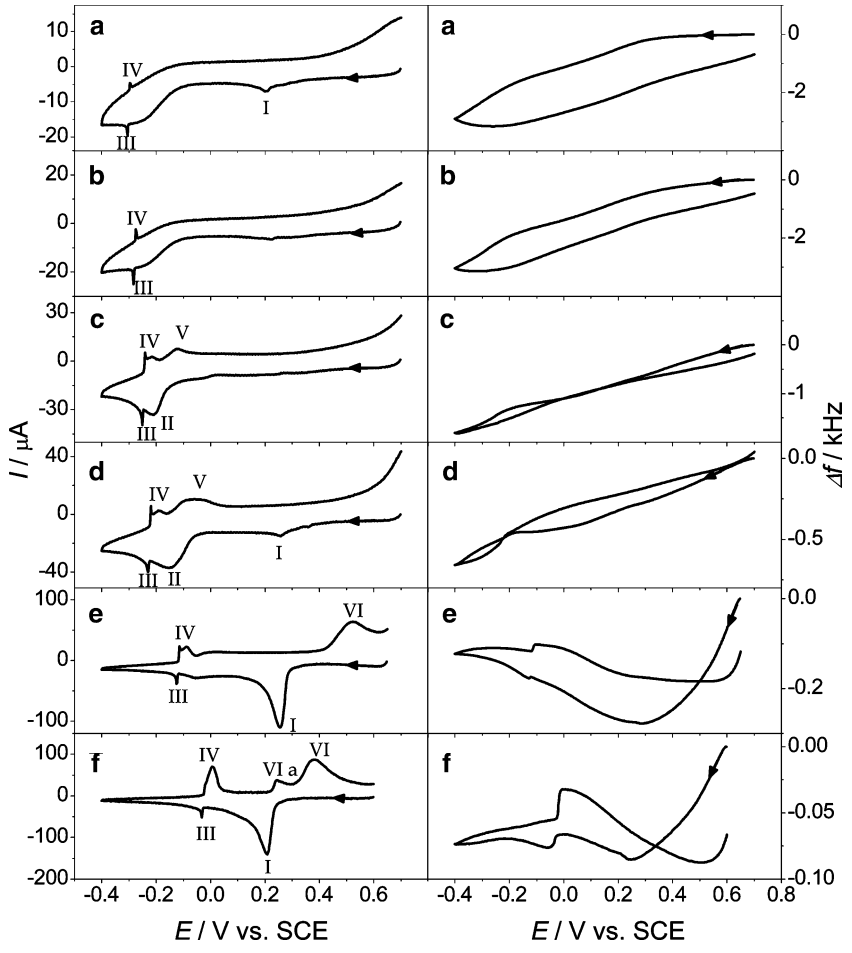

Fig. 6 Cyclic voltammograms and the simultaneously obtained frequency responses obtained for $RuCl_3$ in the presence of LiCl solutions of different concentrations: 0.1 **a**, 0.2 **b**, 0.5 **c**, 1 **d**, 6 **e**, and 12 mol dm^{-3} **f**. Scan rate: 10 mV s^{-1}

The effect of electrolyte concentration

Figure 6 shows the cyclic voltammograms and the respective EQCM frequency curves obtained for the same $RuCl_3$ microcrystals in the presence of LiCl electrolyte of different concentrations between 0.1 mol dm^{-3} and 12 mol dm^{-3}. A comparison with the cyclic voltammogram displayed in Fig. 1 reveals that at high enough LiCl concentrations the reoxidation fully takes place at potentials less than 0.6–0.7 V as a consequence of the shift of the peak potential, E_{pa}(VI) into the direction of less positive values. The characteristic features regarding the concentration dependence are similar in all the electrolytes studied, therefore, only the curves obtained for LiCl are shown. LiCl is very soluble in water, consequently the widest range of concentration can be studied. With increasing concentrations, peak I becomes more positive until ca. 1 mol dm^{-3} and then moves oppositely. Peak VI shifts into the direction of lower potentials, while peaks III and IV move oppositely.

At concentrations higher than 0.5 mol dm^{-3} waves III and IV split, however, the double peaks disappear again at 12 mol dm^{-3}, the sharp peak merges into the increasing other peak and becomes a shoulder. At 12 mol dm^{-3} LiCl, a prepeak (VI a) appears during the reoxidation. The mass changes reveal the more complex nature of the redox transformations.

The most important observation is that the magnitude of the reversible mass change decreases with increasing concentrations. From 0.1 mol dm^{-3} to 1 mol dm^{-3} the picture is relatively simple as much as during the reduction a mass increase occurs. In the region of peak I the frequency starts to decrease which continues even more intensively at peak III. The opposite tendency can be observed during the reoxidation. At higher concentrations, as shown in Fig. 6, a very rapid mass increase occurs at the beginning of the negative-going scan, then at peak I—contrasted with the behavior in dilute solutions—the surface mass decreases. Simultaneously with peak III, a rapid mass decrease takes place which has a counterpart at peak IV. During reoxidation between ca. 0 and 0.5 V the mass loss is regained, however, at the end of the cycle the frequency starts to increase, and it continues at 0.6 V by holding the potential at this value. The rapid mass increase in the beginning of the cathodic cycle is in connection with the mass loss at potentials higher than 0.6 V. In order to investigate this effect we extended the positive potential limit while using 0.2 mol dm^{-3} LiCl. As it can be seen in Fig. 7 another oxidation processes are superimposed on the reoxidation investigated so far, and the species

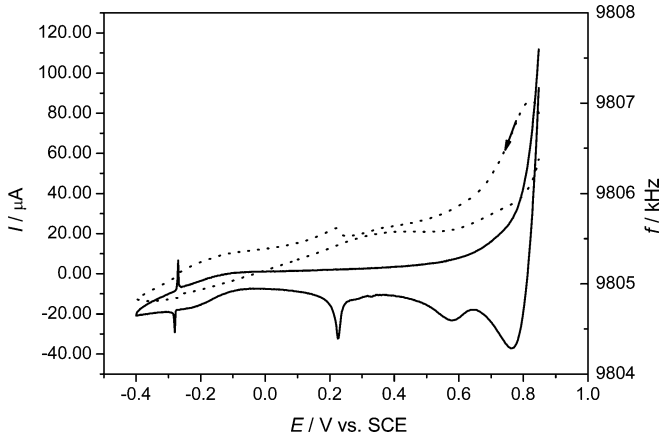

Fig. 7 The effect of the extension of the positive potential limit on the cyclic voltammogram (*continuous line*) and the frequency response (*dotted line*) obtained for an $Au|RuCl_3$ system in the presence of 0.2 mol dm^{-3} LiCl. Scan rate: 5 mV s^{-1}

formed at 0.8 V show the reduction waves at 0.76 and 0.58 V. The study of the pure, uncoated gold electrodes in this solution revealed that the dissolution of gold starts at 0.8 V, i.e., the further oxidation of Ru(III) species takes place simultaneously with the latter process. However, the rather high mass changes in this potential region are not due to the dissolution and deposition of gold since during the reoxidation after a substantial mass gain, the mass decrease starts at potentials higher than 0.6 V at 1 mol dm^{-3} LiCl (Fig. 6d, e, and f). Furthermore, no sharp increase of current can be observed which is characteristic to the metal dissolution, and which is even more important so as no reduction waves in the potential region 0.8 V–0.5 V (see Fig. 7) appear during the negative-going scans. Therefore, a formation of Ru(IV) containing compound has to be assumed. The reduction of this, Ru(IV) containing compound, is accompanied with a rather high mass increase. The "overoxidation" is reversible, returning the usual potential limits the layer behaves as before. The results on Figs. 6 and 7 also reveal that the different mass excursions in dilute and concentrated solutions, respectively, are not related to the "overoxidation" because in 0.2 mol dm^{-3} LiCl the microcrystals behave regularly regarding the mass change in the course of further reduction and reoxidation, and the gold dissolution, if any, does not affect the voltammetric response of the Ru-containing microcrystals.

The frequency-charge curves are shown in Fig. 8. As it has already been pointed out, Q increases with the electrolyte concentration, while the mass change drastically decreases. It follows that the apparent molar mass of the incorporating species decreases, from ca. 550 to 206 after peak I and from ca. 329 to 88 after peak III in the concentration range between 0.1 mol dm^{-3} and 0.5 mol dm^{-3}. At high concentrations from the mass

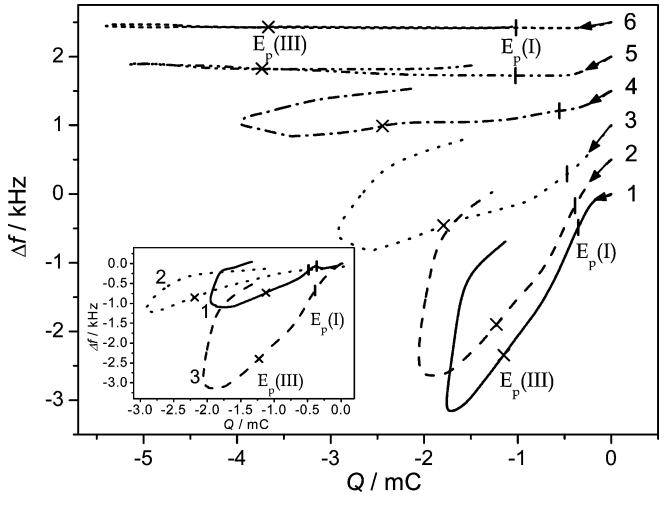

Fig. 8 The frequency changes (Δf) versus charged consumed (Q) curves as a function of the concentration of LiCl solutions: (*1*) 0.1, (*2*) 0.2, (*3*) 0.5, (*4*) 1, (*5*) 6, and (*6*) 12 mol dm^{-3}. Data presented in Fig. 6 are used for the construction of the plots. Insert: Δf versus Q curves for the same electrode in the presence of LiCl after experiments in 0.2 mol dm^{-3} KCl (*1*), after 0.2 mol dm^{-3} CsCl (*2*), and following the study in 0.1 mol dm^{-3} LiCl (3). Waves I and III are indicated on the *plots*

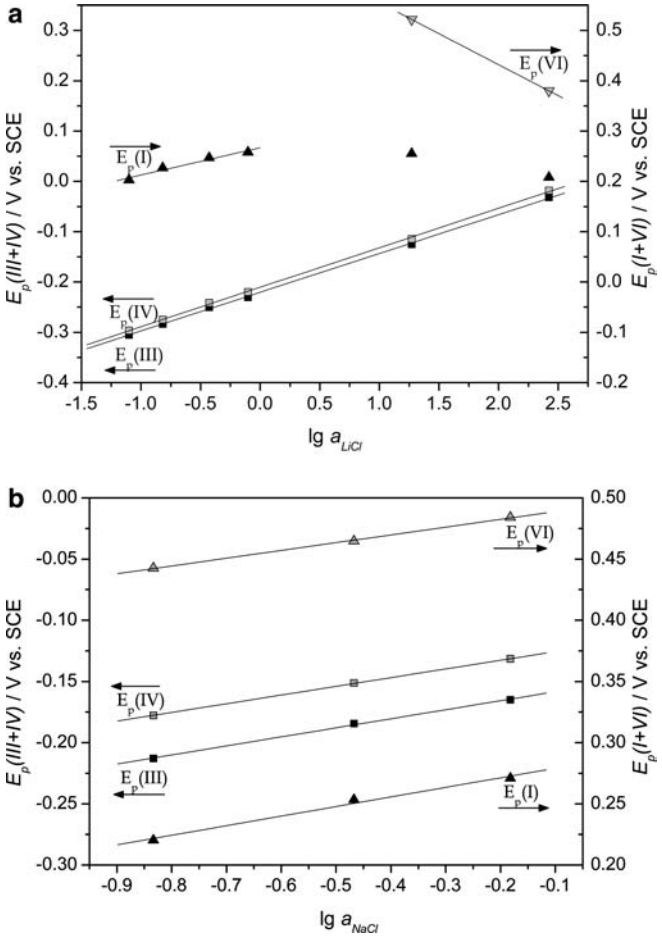

Fig. 9 The variation of the peak potentials as a function of the relative activity of **a** LiCl and **b** NaCl electrolytes. Scan rate: 5 mV s^{-1}

decrease after wave I M_{app}~20 (6 *M* LiCl) can be derived.

The variation of the peak potentials as a function of concentration is also instructive regarding the nature of the electrode reactions. Figure 9 shows the plot of the peak potentials as a function of the relative activity of the electrolyte [45, 46].

In dilute salt solutions $dE_p(I)/d\log a_{MX}$ and $d E_p(VI)/d\log a_{MX}$ values are equal to 64 ± 10 mV/decade as seen in Fig. 9. The same result has been obtained also under acidic conditions when HCl solutions were used [18]. At high concentrations E_p(I and VI) values decrease with increasing a_{MX} or c_{MX}. This effect is related to the change of the electrode reaction. It has been established that ruthenium (III) forms a variety of chloro complexes of the type $[Ru^{III}\ (Cl^-)_m\ (H_2O)_n]^{(3-m)}$ where $m = 1$–6, $n = 5$–0, and $m + n = 6$ [1, 47]. The equilibria existing for the various ruthenium (III) chloro-aqua species [47], as well as the redox reactions are shown in Scheme 1. For the sake of simplicity in Scheme 1 we did not display mixed valence forms which likely exist [1, 18]. The composition of mixed valence complexes is essentially equivalent with that of the compounds (phases) formed via intercalation reactions. Such a scheme of redox transformations is also presented in Scheme 1 [38, 39].

valence oligomers and polymers has also been described [1, 47]. Furthermore, we should not exclude that some kind of ruthenium(IV) oxide/hydride species, mixed ligand oxo derivates are also formed in the potential region 0.6–0.7 V [10, 12, 48–50]. The reduction of the oxides gives a wave around 0.2 V, however, in this case other reduction peaks also appear at higher potentials [49, 50]. Because the exact nature of these ruthenium compounds are unknown and the literature references are rather contradictory, first we will try to explain our observations by considering the well-established ruthenium (III, II) chloro-aqua complexes.

The positive shift of E_p(I) with increasing concentrations that was observed in dilute solutions is in accordance with reactions in which cations participate in K^+/e^- 1:1 ratio. However, the apparent molar mass calculated (Table 1) showed a decreasing tendency with increasing cationic molar mass. This observation can be explained by the flux of water molecules assuming that the small lithium ions enter together with their hydration sphere, while in the case of bulky ions water molecules (that exist in the form of structural water within the microcrystals [1]) leave the surface layer. It means that the values of *x*, *y*, and *z* in Scheme 1 depend on the nature of ions, i.e., their hydration number and size. The

Scheme 1 The redox transformations of Ru(III) chloro-aqua complexes and the intercalation reactions via electron/ion + solvent transfer

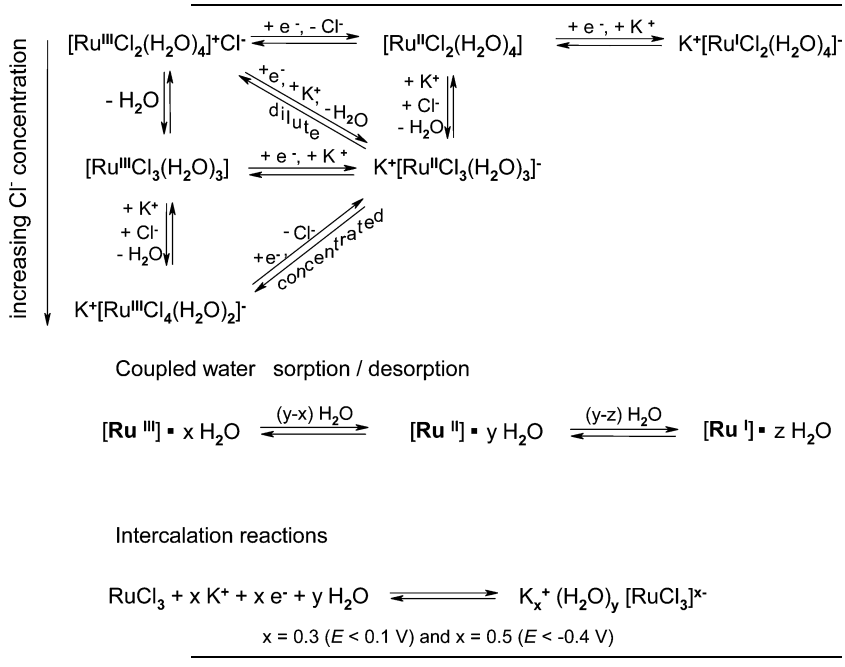

The main difference that the model based on complexes allows the variation of the Ru|Cl ratio, as well. At low Cl^- concentrations mostly the lower chloro complexes exist, while at high Cl^- concentrations the higher chloro complexes exist and take part in the electrode reactions. Contrary to the solution situation, in the case of microcrystals attached to the gold surface we should consider also the counterions. However, the actual situation may be much more complicated. Ru(II) complexes can undergo further transformations. Formation of mixed

complex mechanism and the role of the structural changes are manifested in several phenomena. Such effects are the slight mass decrease at wave I before a continuous mass increase (see Figs. 1, 4) or the disappearance of this effect and the variation of the magnitude of the $\Delta m/Q$ ratio that depend on the prehistory of the sample (Figs. 4, 8). It is also likely that equilibria exist between different Ru(III) complexes and between different Ru(II) complexes within the layer. It follows that while the dominating process is the incorporation of

cations without or together with a loss of water, in a smaller degree desorption of chloride ions also occurs during the same reduction step. As the electrolyte concentration increases the mass increase before peak I becomes more and more pronounced, however, the total mass excursion becomes much smaller than that in dilute solutions (Figs. 6, 8). At high concentrations at the first reduction wave a mass decrease starts which is just the opposite of that observed in dilute solutions. The mass increase at the beginning of the negative-going scan may be capacitive in nature since no substantial charge was consumed. The concentration dependence supplies an additional argument regarding the importance of water sorption/desorption effect, since at higher Cl^- concentrations the complex equilibria are shifted to the higher chloro complexes, which would be in accordance with higher and not with smaller mass change in as much as in this case cation sorption is the expected process during reduction. However, taking into account the decreasing water activity at high LiCl concentrations the phenomena observed become more understandable. In 12 mol dm^{-3} LiCl the full hydration of Li^+ ions is impossible since the total number of the available H_2O molecules per Li^+ ions is less than 5. The shift of E_p(I) and E_p(VI) into the direction of lower potentials at high a_{LiCl} cannot be explained in this way. The possible explanation is that during the reduction lower Ru(II) chloro complexes are formed, i.e., instead of the incorporation of cations, anions leave the surface layer (see Scheme 1).

The effect of pH

As seen in Fig. 10 the decrease of pH causes a substantial shift of E_p(VI) into the direction of lower potentials. E_p(I) is rather insensitive to pH, a positive shift can be observed only at low pH values, while the pair of waves III and IV moves into the direction of higher potentials. A substantial increase of the electroactivity of the microcrystals with decreasing pH can be observed. It is certainly not related to the increasing electrolyte concentration, since the concentration increase in 0.1 mol dm^{-3} LiCl + x mol dm^{-3} HCl is negligible between pH 7 and pH 2, and at pH 1 the total concentration is still only 0.2 mol dm^{-3}, which according to the results presented in Fig. 6 affects both the voltammetric and EQCM frequency changes only slightly. The impact of pH on the mass change is even more remarkable. The frequency changes are much smaller in more acidic solutions, and at peak I the direction of the mass change varies, the mass increase observed at higher pH values turns into mass decrease (see also Ref. [18]). During further reduction the mass of the surface layer increases, then decreases again including an abrupt change at peak III (Fig. 11). However, with increasing acid concentration the pattern of the frequency changes varies in this potential region. In neutral solutions at peak III the frequency suddenly decreases, which is followed by either a continuous frequency decrease or a slight increase depending on the electrolyte concentration. During reoxidation at peak IV a mass decrease occurs which is steep at high concentrations, and followed by a frequency decrease. At low concentrations the frequency increase is less distinct, the frequency continuously increases, and reaches the initial value after the complete reoxidation. Acidifying the solution causes rather surprising phenomena. At peak III, after a small frequency decrease, a fast frequency increase occurs, however, at peak IV the frequency increases again in a step-like manner. Consequently, during continuous cycling the surface mass continuously decreases, although the magnitude of the frequency changes remains the same and the characteristics of the frequency-potential curves do not change as it can be seen in Fig. 12. Such type of frequency change usually means the dissolution of the material attached to the metal substrate. However, in the case of dissolution the electroactivity (the charge consumed) also continuously

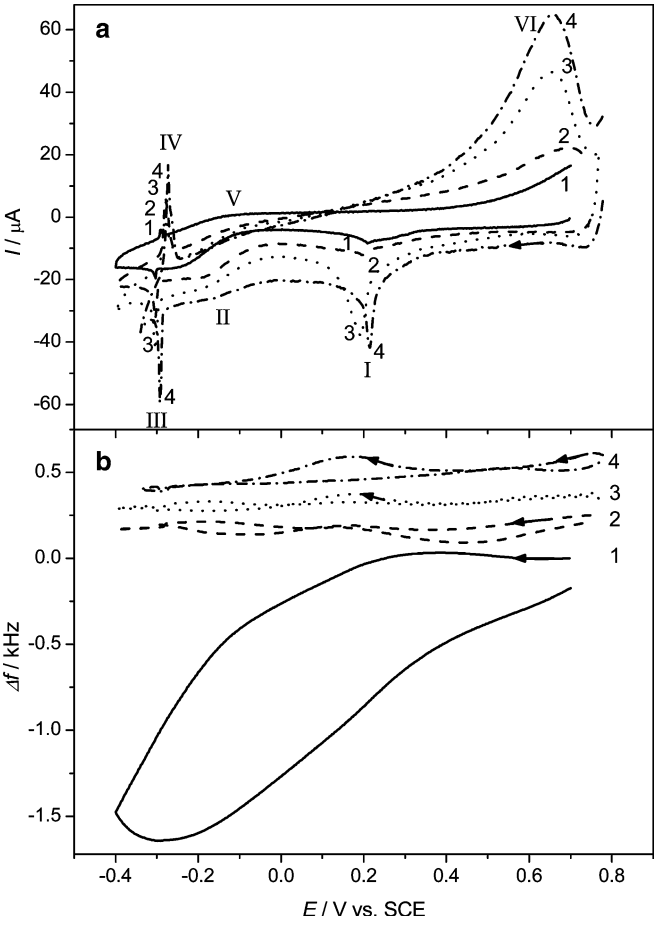

Fig. 10 Cyclic voltammograms **a** and the respective frequency curves **b** for an Au|$RuCl_3$ electrode in the presence of 0.1 mol dm^{-3} LiCl + x mol dm^{-3} HCl. The pH of the solution was 7 (*1*), 3 (*2*), 2 (*3*), and 1 (*4*), respectively. Scan rate: 5 mV s^{-1}

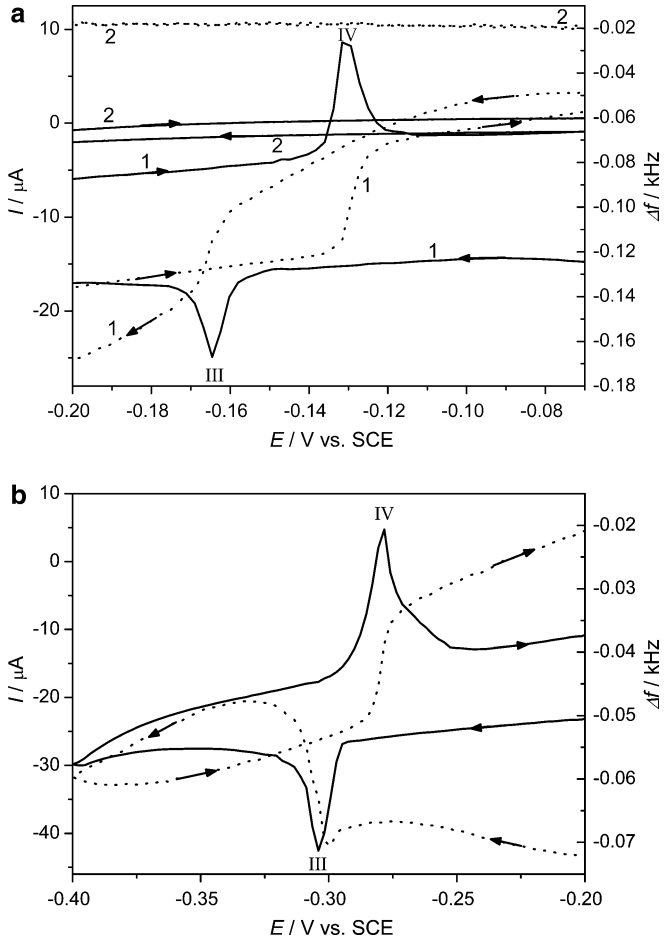

Fig. 11 Enlarged portions of the cyclic voltammograms (*continuous lines*) and the frequency responses (*dotted lines*) in the potential region of waves III and IV, **a** 1 mol dm^{-3} NaCl, **b** 0.1 mol dm^{-3} LiCl + 0.1 mol dm^{-3} HCl. For the sake of comparison the responses obtained for Au|$RuCl_3$ (*curves 1*) and for pure gold (*curves 2*), respectively, are also displayed. Scan rate:5 mV s^{-1}

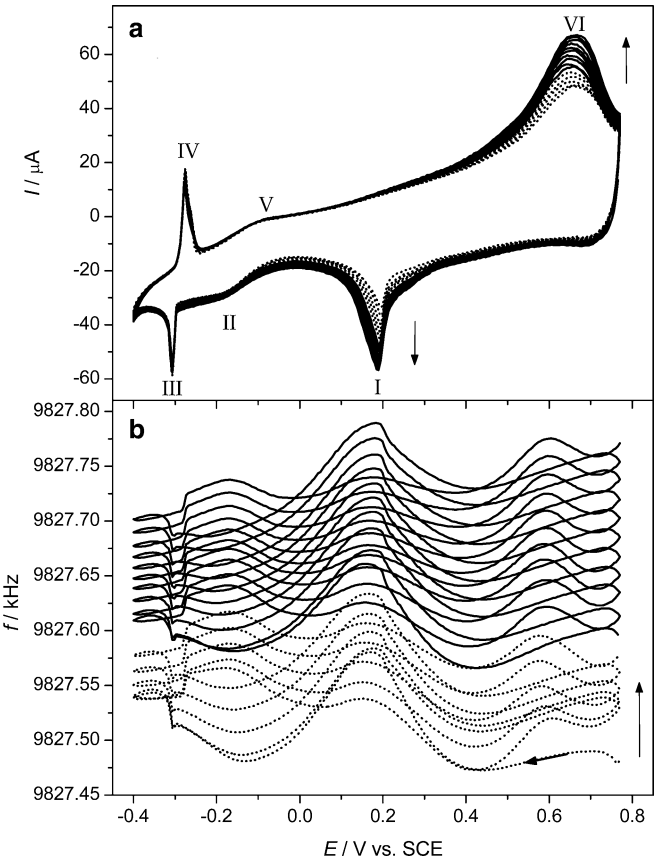

Fig. 12 Consecutive cyclic voltammograms **a** and the simultaneously obtained frequency responses **b** for an Au|$RuCl_3$ electrode after replacing 0.1 mol dm^{-3} LiCl + 0.001 mol dm^{-3} HCl (pH 3) solution for 0.1 mol dm^{-3} LiCl + 0.01 mol dm^{-3} HCl (pH 2). Scan rate: 10 mV s^{-1}. First five cycles (*dotted line*), next ten cycles (*continuous line*)

decreases. In Fig. 12 just the opposite can be seen, by varying the pH from 3 to 2, the electroactivity steadily increases. Therefore, the mass loss is not a consequence of the dissolution of the microcrystals, it should be related to the exchange (loss) of certain mobile species, i.e., to dehydration or anion (ligand) and/or cation desorption (exchange) due to the transformation of the complexes (crystal structure). This conclusion is supported by the fact that by increasing the pH of the solution the original behavior can be regained.

The nature of waves III and IV is certainly interesting. A closer inspection of the cyclic voltammograms and the mass changes reveals that waves III and IV are superimposed on other redox processes. The drawn-out waves (labeled as waves II and V in Figs. 10, 12) belong to the further reduction of the bulk microcrystals. The sharp waves III and IV (half-widths ca. 10 mV) are most likely due to a redox reaction at the gold/microcrystal interface. From the charge consumed $(5 \pm 1) \times 10^{-10}$ mol cm^{-2} and $(1 \pm 0.8) \times 10^{-9}$ mol cm^{-3} can be calculated in the cases of NaCl and HCl/LiCl systems, respectively.

From the $\Delta f/Q$ values $M_{app} = 850 \pm 50$ (reduction), $M_{app} = 500 \pm 20$ (oxidation), and $M_{app} = 130 \pm 10$ (reduction), $M_{app} = 80 \pm 10$ (oxidation) can be calculated for NaCl and HCl/LiCl systems, respectively. In this case only the charge under the peak, i.e., neglecting the "background current" which probably belongs to other process, has been taken into account. The rather high values might be a consequence of a phase transition and the strain in the surface layer and/or the extensive hydration/dehydration and surface structural changes [18, 40, 41].

Another possible explanation is an intercalation process different from the simple topotactic intercalation process that has been described in the literature [38, 39, 51–55]. For instance, the intercalated cations can occupy the empty places [19, 20] in the metallic sheets.

We have also considered the underpotential deposition (upd) of alkali metal ions, since such a process was suggested for Na^+ and Cs^+ ions on gold recently [56]. However, we have to reject this explanation, since neither the background current nor the frequency change

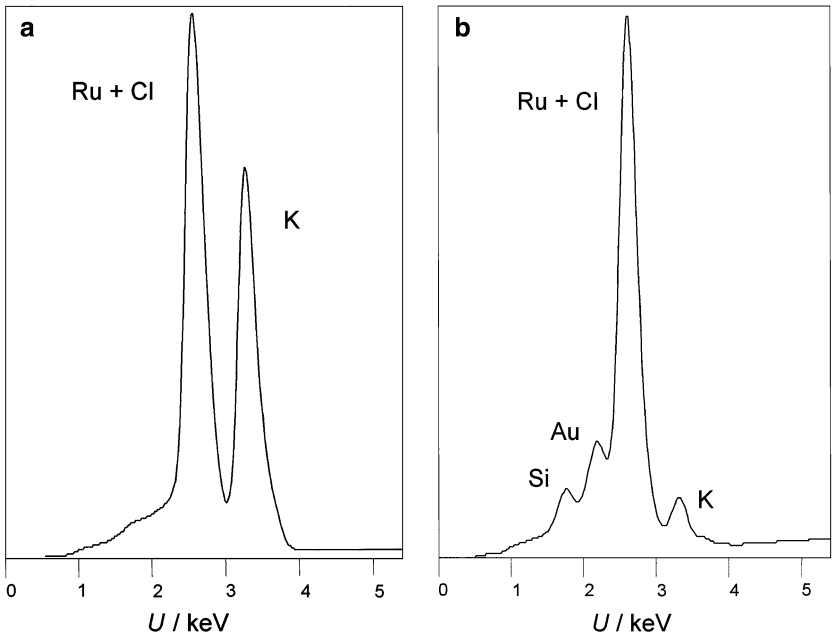

Fig. 13 TXRF spectra of **a** blend of $RuCl_3$ + KCl with 1:1 mass ratio, **b** the product of the cathodic reduction at −0.4 V. The electrolysis time was 10 min. Mo-tube was operated at 50 kV and 38 mA. Integration time was 3,000 s. At $U = 2.6$ keV the peaks of Ru(L_α + L_β) and Cl(K_α) appear together, the K(K_α) line is at 3.3 keV. For the calibration Ru(K_α) line at 19.3 keV was also used. The Au (M_α + M_β) line that appears at 2.15 keV is originated from the gold electrode, the Si line at 1.7 keV is due to the sample holder

indicate the occurrence of any upd process (see the respective curves on Figs. 11a, 1 and 3).

Complex formation or intercalation

Intercalation chemistry of α-RuCl has been reported with the insertion of simple cations and neutral polar molecules. It has been established that cations can be intercalated reductively or through ion-exchange, while neutral polar molecules can be incorporated through solvent exchange [39, 52]. It has also been shown that the lamellar structure of the inorganic host is preserved, however, the separation of the $RuCl_3$ layers somewhat increases [39, 52]. In these papers [38, 39, 51, 52] mixed-valent, non-stochiometric ruthenium compounds with a general formula $M^{n+}{}_{x/n}(H_2O)_y[RuCl_3]^{x-}$ have been considered where M^{n+} are metal ions or in acid solutions: H_3O^+. For instance, $K_x{}^+(H_2O)[RuCl_3]^{x-}$ or $(H_3O)_x{}^+(H_2O)_y[RuCl_3]^x-$ with $x_{max} = 0.5$ has been proposed [38]. It has been verified that the structures of hydrated phases with alkali metals are related to the hydration enthalpies of the guest cations and are dependent upon the concentration of the contacting electrolyte [39]. It has been found that Li insertion increases the electrical conductivity. The conductivity of Li_xRuCl_3 ($x \sim 0.2$) is about three orders of magnitude higher than that of pristine α-$RuCl_3$ [52]. The intercalation model is supported at least for waves III/IV and in some cases for wave I, since such voltammetric peaks with small half-height widths have been found for lithium intercalation in graphite film electrodes [53–55].

On the basis of cyclic voltammetry and piezoelectric microgravimetry it is not possible to distinguish between the two models. The complex formation is supported by the fact that both Ru(III) and Ru(II) chlorides easily form chloro-aqua complexes in chloride containing aqueous media [1–4, 7, 8] and several complexes have been prepared. On the other hand, there are strong evidences (e.g., X-ray diffraction [52], scanning electron microscopy [51]) for the intercalation process. In the lamellar structure of α-$RuCl_3$, layers composed of hexagonal sheets of Ru atoms are sandwiched between two hexagonal sheets of Cl atoms with ABC stacking. The intercalated ions (compensating the negative charge of $RuCl_3^{x-}$ after reduction) and water or other neutral molecules are situated between the layers causing an increase of the interlayer distance. Nevertheless, it might be assumed that some kind of complex formation occurs even in this case. Both ideas involve mass changes due to the sorption/desorption of ions and water molecules during the redox processes. In the complex model the number of ligands are fixed, and H_2O may be present as a ligand and also in the form of structural water. In the intercalation model, in principle, chloride ions belong to $RuCl_3$ and H_2O molecules occupy the interlayer space together with the cations. It is not exactly true because in dilute acidic solutions, an amorphous colloid phase has been formed and the chemical reduction has been explained by the incorporation of anions [39]. However, the most significant difference is the extent of reduction. Its indicator is the Ru/K ratio.

The Ru/K ratio has been determined by the help of TXRF spectrometry. The TXRF spectra obtained for Ru, pristine $RuCl_3$, $RuCl_3$ + KCl 1:1 blend and [$RuCl_3$] samples after electrolysis in 0.2 mol dm^{-3} KCl. Illustrative spectra are presented in Fig. 13. From each area under the characteristic peaks, which reflects the mass of the species in the sample, the amount of Ru, Cl, and K was calculated taking into account the respective sensi-

tivity factors. The molar ratios were determined by using these values and the molar masses of the elements. The K/Ru ratio has been found 0.3 ± 0.15 in the potential range studied. The actual value strongly depends on the duration of the electrolysis. The smaller values for the K/Ru ratio were found when the sample was thick and the electrolysis was not exhaustive. In this case the outer part of the sample remained intact in the form of $RuCl_3$, therefore, the smaller K^+ content is understandable. This finding is in accordance with the results of the intercalation reactions [39]. It has been reported [39] that during galvanostatic cathodic reduction in the potential region between 0.4 V and 0.2 V, a two phase system develops with the coexistence of $RuCl_3$ and $K^+_{1/3}(H_2O)_y[RuCl_3]^{1/3-}$, while between 0.2 V and −0.4 V a single nonstoichiometric phase containing high amount of water is formed where $0.3 < x < 0.38$. With further reduction at $E < -0.4$ V, a phase with a composition of $K_{0.5}(H_2O)_y[RuCl_3]^{0.5-}$ was formed, and it was established that the upper limit is not higher than $x = 0.5$. It has been explained in terms of the electronic transport properties, in as much as the mixed valence phases have a high electronic conductivity, while an electrochemical reduction beyond a charge transfer corresponding $x = 0.5$ creates a thin electronically insulating interface blocking further electron transport via the $RuCl_3$ layers [39]. By the help of this model most of our findings can be explained except the concentration dependence of the peak potentials of waves I and VI at high concentrations (see Fig. 9a) and the nature of waves III and IV. Therefore, the reaction scheme assuming the formation of different complexes (Scheme 1) may also be operative, since it can supply an explanation for the behavior at high electrolyte concentrations providing a formation of mixed valence compounds, e.g., $[Ru^{III}Cl_3(H_2O)_3]K^+[Ru^{II}Cl_3(H_2O)_3]^- \bullet 0.5(x+y)\ H_2O$.

Conclusions

The robustness of α-$RuCl_3$, immobilized on a gold surface in neutral or acidic aqueous media, allows the study of its redox transformations. $RuCl_3$ microcrystals can be reduced in several steps in the presence of aqueous solutions of $M^+ X^-$ electrolytes. The peak potentials and the changes of the surface mass strongly depend on the nature and the concentration of the electrolyte. The results can be elucidated by the formation of complexes or intercalation compounds which contain mixed valence $Ru^{III/II}$-centers, Cl^- ions, univalent metal ions (M^+) or H^+ ions, and water molecules, the ratio of which depends on the potential and the solution composition.

During reduction, M^+ ions enter the layer. The highly hydrated small ions transport their hydrate sphere, while the insertion of large size ions causes a desorption of water molecules. The exchange of chloride ions is also likely at high electrolyte concentrations. The redox transformations are accompanied with structural changes of the microcrystals.

Acknowledgements Financial support by the National Scientific Research Fund (OTKA T046987) is gratefully acknowledged.

References

1. Cotton FA, Wilkinson G, Murillo CA, Bochman M (1999) Advanced inorganic chemistry. Wiley, New York, pp 1010–1039
2. Livingstone SE (1973) In: Bailar JC, Emeléus MJ, Nyholm R, Trotman-Dickenson AF (eds) Comprehensive Inorganic Chemistry, vol 3. Pergamon Press, Oxford, pp 1163–1370
3. Chandret B, Sabo-Etienne S (1994) In: King RB (ed) Encyclopedia of inorganic chemistry, vol 7. Wiley, Chichester
4. Appelbaum L, Heinrichs C, Demtschuk J, Michman M, Oron M, Schäfer HJ, Schumann H, Organomet J (1999) Chem 592:240
5. Trasatti S (2000) Electrochim Acta 45:2377
6. Latimer WM (1952) The oxidation states of the elements and their potentials in aqueous solutions. Prentice-Hall, Englewood Cliffs, p 228
7. Llopis JF, Tordesillas IM (1976) In: Bard AJ (ed) Encyclopedia of electrochemistry, vol 6. Marcel Dekker, New York, p 277
8. Colom F (1985) In: Bard AJ, Parsons R, Jordan J (eds) Standard potentials in aqueous solution. Marcel Dekker, New York, p 413
9. De Benedetto GE, Guascito MR, Ciriello R, Cataldi TRI (2000) Anal Chim Acta 410:143
10. Kasem K, Steldt FR, Miller TJ, Zimmerman AN (2003) Microporous Mesoporous Mat 66:133
11. Chen SM, Hsueh SH (2004) J Electroanal Chem 566:291
12. Kulesza PJ (1987) J Electroanal Chem 220:295
13. Scholz F, Meyer B (1998) In: Bard AJ, Rubinstein I (eds) Electroanalytical Chemistry, vol 20. Marcel Dekker, New York, p 1
14. Grygar T, Marken F, Schröder U, Scholz F (2002) Coll Czech Chem Commun 67:163
15. Fiedler DA, Scholz F (2002) In: Scholz F (ed) Electroanalytical Methods Ch II 8. Springer, Berlin Heidelberg New York, pp 201–222
16. Bond AM, Marken F, Williams CT, Beattie DA, Keyes TE, Forster RJ, Vos JG (2000) J Phys Chem 104:1977
17. Ramaray R, Kabbe C, Scholz F (2000) Electrochem Commun 2:190
18. Inzelt G, Puskás Z (2004) Electrochem Commun 6:805
19. Pollini I (1994) Phys Rev B 50:4
20. Pollini I (1996) Phys Rev B 53:19
21. Mott NF (1961) Philos Mag 6:287
22. Wilson JA (1985) In: Edwards PP, Rao CN (eds) The Metallic and Nonmetallic States of Matter. Taylor and Francis, London, pp 215–260
23. Fehér K, Inzelt G (2002) Electrochim Acta 47:3551
24. Inzelt G (2003) J Solid State Electrochem 7:503
25. Inzelt G, Puskás Z (2004) Electrochim Acta 49:1969
26. Varga I, Bohlen A, von Klockenkämper R, Záray G (2000) Microchem J 67:265
27. Varga I, Rierpl E, Tusai A (1999) J Anal At Spectrom 14:881
28. Vittal L, Jayalakshim M, Gomathi H, Prahakara Rao G (1999) J Electrochem Soc 146:786
29. Schneemeyer LF, Spengler SE, Murphy DW (1985) Inorg Chem 24:3044
30. Bácskai J, Martinusz K, Czirók E, Inzelt G, Kulesza PJ, Malik MA (1995) 385:241
31. Retter U, Widmann A, Siegler K, Kahlert H (2003) J Electroanal Chem 546:87
32. Chen SM (2002) J Electroanal Chem 521:29
33. Pournaghi-Azar MH, Dastangoo H (2002) J Electroanal Chem 523:26
34. Engel D, Grabner EW (1985) Ber Bunsenges Phys Chem 89:982
35. Chen SM, Chan CM (2003) J Electroanal Chem 543:161

36. Cui X, Hong L, Lin X (2002) J Electroanal Chem 526:115
37. Malik MA, Horányi G, Kulesza PJ, Inzelt G, Kertész V, Schmidt R, Czirók E (1998) J Electroanal Chem 452:57
38. Schöllhorn R, Steffen R, Wagner K (1983) Angew Chem 95:559
39. Steffen R, Schöllhorn R (1986) Solid State Ionics 22:31
40. Evans CD, Chambers JQ (1994) Chem Mater 6:454
41. Hepel M, Janusz W (2000) Electrochim Acta 45:3785
42. Scholz F, Lovric M, Stojek Z (1997) J Solid State Electrochem 1:134
43. Suárez MF, Bond AM, Compton RG (1999) J Solid State Electrochem 4:24
44. Puskás Z, Inzelt G (2004) J Solid State Electrochem 8:828
45. Robinson RA, Stokes RH (1959) Electrolyte solutions. Butterworths, London, pp 491–504
46. Handbook of Chemistry and Physics (1977) Weast RC (ed) CRC Press, Cleveland, Ohio, p D-234
47. Taqui Khan MM, Ramachandraiah G, Prakash Rao A (1986) Inorg Chem 25:665
48. Trasatti S, Kurzweil P (1994) Platinum Met Rev 38:46
49. Wang JX, Marinkovic NS, Zajonz H, Ocko BM, Adzic RR (2001) J Phys Chem B 105:2809
50. Vericat C, Wakisaka M, Haasch R, Bagus PS, Wieckowski A (2004) J Solid State Electrochem 8:794
51. Wang L, Brazis P, Rocci M, Kannewurf CR, Kanatzidis MG (1998) Chem Mater 10:3298
52. Wang L, Rocci-Lane M, Brazis P, Kannewurf CR, Kim YI, Lee W, Choy JH, Kanatzidis MG (2000) J Am Chem Soc 122:6629
53. Levi MD, Aurbach D (1997) J Electroanal Chem 421:79
54. Levi MD, Levi EA, Aurbach D (1997) J Electroanal Chem 421:89
55. Levi MD, Aurbach D (1997) Electrochim Acta 45:167
56. Ohmori T, El-Deab MS, Osawa M (1999) J Electroanal Chem 470:46